A Novel Test Method for Real-time Magnetic Flux Measurement of Power Transformers

Ying ZHANG[1], Dangdang DAI[2], Jing ZHANG[3], Xiaoli LIU[4], Xuxuan CHEN[5]
[1]*Electric Power Research Institute of Guizhou Power Grid Co., Ltd., China*
[2]*Information and Communication Center, State Grid Hubei Electric Power Co., Ltd, China*
[3]*School of Electrical Engineering, Guizhou University, China*
[4]*State Grid Electric Power Research Institute, China*
[5]*Wuhan University of Science and Technology, China*
zhangjing@gzu.edu.cn

***Abstract*—Optimizing magnetic flux distribution in iron cores is very important in the transformer design. It can affect whether the iron cores of transformers are saturated or not in severe conditions. If saturated, the transformer will overheat and generate harmful harmonics to the grid. The measurement of the dynamic magnetic flux is an effective method to observe the behavior of transformers and ensure their safety. However, there are limited methods to measure the magnetic flux in real-time. In this paper, a novel test method based on a special transformer design is proposed. The new design integrates an additional bypass iron core which shares a partial magnetic path with the main core. By injecting high-frequency signals into the attached coil of the bypass core, the measured signals reflect the trend of the magnetic flux variation in the main core over time. To improve the accuracy of the derived measured data, the Empirical Mode Decomposition algorithm is also used to diminish the noise without additional designs in the signal acquisition circuit. The proposed method is modeled and tested, and the results show that this method can dynamically measure the magnetic flux in the transformer.**

***Index Terms*—magnetic circuits, power transformers, empirical mode decomposition, test equipment, finite element analysis.**

I. INTRODUCTION

Transformers and inductors are widely used in nowadays power grids and are much more important than ever because many of them are core devices in power electronic systems. Magnetic circuits, as the key components of transformers and inductors, are of great concern for electrical engineers [1]. Ferromagnetic materials used in the magnetic component are highly non-linear and can be driven into saturation if design specifications are not optimal, especially in severe conditions such as overload, inrush currents, geomagnetically induced currents (GIC) and other faults [2-6]. In the above situations, there will be distorted high currents in the main coils, leading to additional power loss and overheating the transformers [7-9]. The DC-bias in iron cores of transformers will also result in reactive power variation and noises [10-12]. Even dielectric materials can be damaged, which results in a more serious short circuit fault and permanent destruction of transformers and inductors.

In order to protect the expensive transformers from being saturated, saturation protection relays are imperatively needed. However, there is a limited method to protect transformers from the saturation due to the lack of effective direct signal gathering of the magnetic strength or the magnetic flux in transformer iron cores [13-15]. At present, it is a common practice to install additional devices, such as capacitive circuits, polarizing cells and neutral linear resistance at the transformer neutral, so as to passively block the transformer from being saturated. These methods are demonstrated on a small network, but for large scale power grid, more flexible and versatile techniques are required [16].

Normally two types of methods can be used to measure the magnetization characteristic (B-H behavior) of the iron core in transformers: the offline measurement or the indirect measurement [8-10]. For offline measurement, Epstein square and single sheet measurement are widely used. Epstein square measurement is shown in Fig. 1. Exist international standards are defined by literature [17, 18]. The limitation of the above methods is that they can not be applied in onsite transformers to measure the dynamic BH behavior of the magnetic materials.

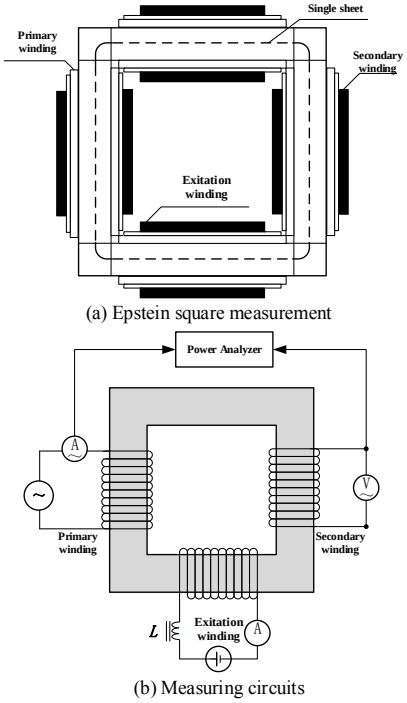

Figure 1. Epstein square measurement

And, indirect measurement is a kind of semi real-time

This work was supported by the Science and Technology Project of China Southern Power Grid Co., Ltd. under Grant No. GZKJXM20160018; the National Natural Science Foundation of China under Grant No. 51867005.

Digital Object Identifier 10.4316/AECE.2019.04004

experiment method based on the electromagnetic induction principle. Before the measurement, important geometry characteristics like the cross-sectional area of the core and the length of the magnetic circuit must be known. By integrating the measured voltage in the secondary winding when the rated voltage is applied on the first winding, magnetic flux density in the iron cores is derived. The indirect measuring method has a delay effect compared with the actual magnetic behavior in the iron cores due to an integral algorithm. Also, to process the measured signals, the method needs specific analog circuits that can not withstand high electrical voltage, so it can hardly be implemented on high voltage transformers measurement and protection applications [19-21].

This paper proposes a novel test method based on a special transformer design. The new design integrates an additional bypass iron core which shares a partial magnetic path with the main core. By injecting high-frequency signals into the attached coil of the bypass core, the measured signals will reflect directly the trend of the magnetic flux variation in the main core over time. Since the amplitude of the measured signals are small, they could be interfaced by noises generated from the injection source whose key components are power electronics. Considering that some effective signals will be filtered if filter circuits are used, the Empirical Mode Decomposition (EMD) algorithm is used here to retain all the information from the measurement. The proposed method is modeled and tested by using a FEM corporate simulation method using Matlab/Simulink.

The paper is organized as follows: The dynamic magnetic flux measurement method is introduced in Section II and the optimal bypass iron cores design is described in Section III. Simulation and test setup demonstrating the proposed technique are presented in Section IV. The signal processing method of the measured data is shown in Section V. The measurement results under DC-bias condition are reported in Section VI and a conclusion and direction for future work are given in Section VII.

II. Dynamic Magnetic Flux Measurement Method

To measure the dynamic magnetic flux in the main core, a bypass core is employed to stick to the main core as close as possible [22]. However, there would still be some air gap between the bypass core and the main core. Therefore, in this research, a special core lamination is designed which will be explained in section IV.

As shown in Fig. 2, the bypass core shares a common path with the main core and the magnetic reluctance value is R_a. When the magnetic reluctance R_m of the main core is changed, the whole magnetic reluctance (R_m+R_a) in the magnetic path will also be affected.

$$R_m = \frac{l_m}{\mu_0 \mu_m A_m} \tag{1}$$

$$R_a = \frac{l_a}{\mu_0 \mu_a A_a} \tag{2}$$

where lm represents the length of the shared magnetic path, la is the length of the bypass magnetic path, μ_0, μ_m, μ_a are the magnetic permeability of vacuum, the main core, and the bypass core. A_m, A_a are the cross-section area values of the main core and the bypass core.

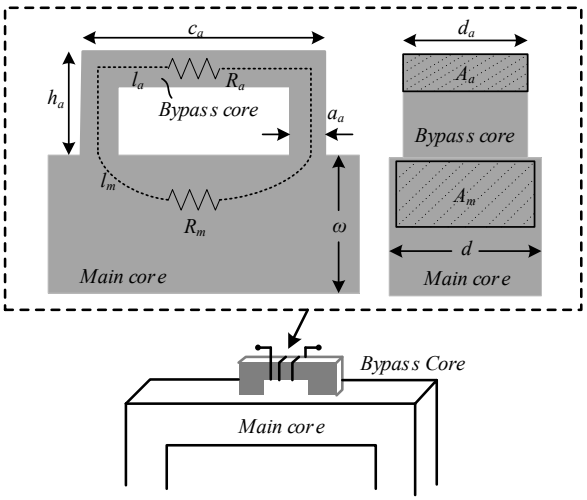

Figure 2. Dynamic magnetic flux measurement methods

If there is no DC-bias magnetic flux in the main core, the total reluctance of the bypass core can be described in,

$$R_{eq} = R_m + R_a \rightarrow \frac{l_{eq}}{\mu_0 \mu_{eq} A_{eq}} = \frac{l_m}{\mu_0 \mu_m A_m} + \frac{l_a}{\mu_0 \mu_a A_a} \tag{3}$$

where leq, μeq, and Aeq represent the equivalent length, permeability and cross-section area of the whole magnetic path.

Finally, the inductance L_{eq} of the coil attached on the bypass coil is as follows,

$$L_{eq} = \frac{0.4\pi N^2 \mu_{eq} A_{eq} \times 10^{-8}}{l_{eq}} \tag{4}$$

III. Optimal Bypass Iron Cores Design

For input signals, because the reactance of the coil on the bypass coil is very small, a high frequency constant current signal is suggested, which will result in an amplified amplitude value of the output voltage.

In order to get a more accurate value of the measured reactance L_{eq}, the bypass iron core also needs optimization. First, the precision η representing the changing rate of the auxiliary coil inductance is defined as,

$$\eta = \frac{L_{eq} - L'_{eq}}{L_{eq}} \times 100\% \tag{5}$$

where L'_{eq} is the coil reactance of the bypass iron core when magnetic permeability of the main core decreases to its half value.

Substitute (1)-(4) into (5),

$$\eta = \frac{1}{2 + \frac{\mu_m A_m l_a}{\mu_a A_a l_m}} = \frac{1}{2 + \frac{R_a}{R_m}} \tag{6}$$

In order to get the largest value of η, or to maximize the sensitivity, the magnetic reluctance R_m of the main core should be much greater than the magnetic reluctance R_a.

FEM simulation is a very powerful tool to study the BH characteristic of transformers [20]. So in this research, the proposed magnetic flux measurement is also modeled using the FEM method, as shown in Fig. 3.

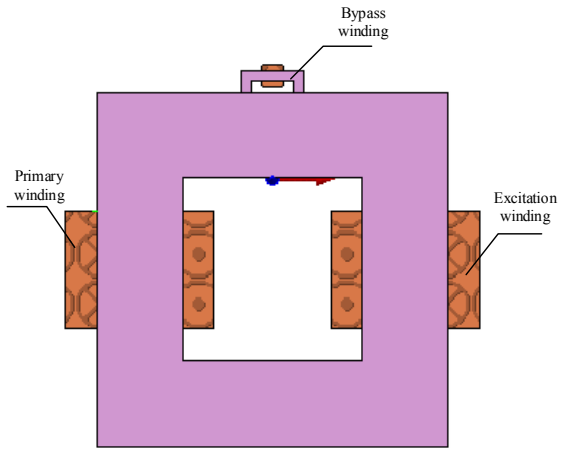

Figure 3. Test platform model of the proposed magnetic flux measurement

The model is used to aid the bypass core design in order to get a high precision of the measured signals. The main design parameters are magnetic permeability μ_a, the width a_a and length C_a of the bypass core. The BH characteristic of the main core is shown in Table I.

TABLE I. THE BH CHARACTERISTIC OF THE MAIN CORE

H(A/m)	B(tesla)
13.56385	0.1644
539.1612	1.2840
1104.598	1.3656
3342.504	1.497782
9259.008	1.6846
20092.84	1.8233
30413.15	1.8888
40408.02	1.917251
60327.86	1.9660
120860	2.0665

In equations (1) and (2), the area and the magnetic permeability of the bypass core should be as large as possible. And the depth width d_a of the bypass core should be close or equal to d of the main core. The value of a_a should be close to the value of ω, but from the simulation a_a/ω=0.1 is good enough to obtain a precise measurement.

However, the length C_a of the bypass core is hard to optimize. If C_a is shorter, the length of the shared magnetic path l_m will decrease, and the R_m value will decrease. If C_a is longer, the length of the magnetic path l_a will increase, and the R_a value will increase. From equation (6), the sensitivity of the value η can hardly be simply defined.

The simulation result comparison of the magnetic flux in the main core when C_a is different is shown in Fig. 4. It shows that when C_a/ω is larger, the shared magnetic flux is greater which will increase the precision of the measurement. But if C_a length is too large, there will be unnecessary flux hitting the other side of the main core. The energy of the measured signals will lose which will decrease the efficiency η. Several simulation tests based on the FEM model are performed. Their results are shown as follows.

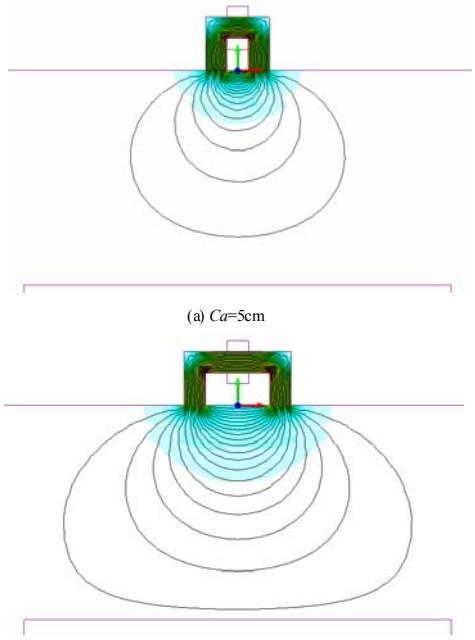

Figure 4. Simulation results comparison of the magnetic flux in the main core when Ca is different

If a_a/ω=0.1, the calculated value of η versus C_a/ω is shown in Fig. 5.

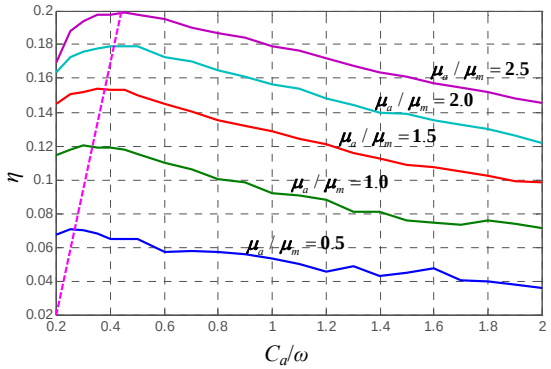

Figure 5. a_a/ω=0.1, the calculated value of η versus C_a/ω

Fig. 5 suggests that the magnetic permeability of the bypass core should be 1 to 2 multiplies of the value of the main core in order to get a higher value of η. When the value of C_a/ω is below 0.4, η will be greater than 0.12.

Fig. 6 shows the η versus C_a/ω when μ_a/μ_m=1.

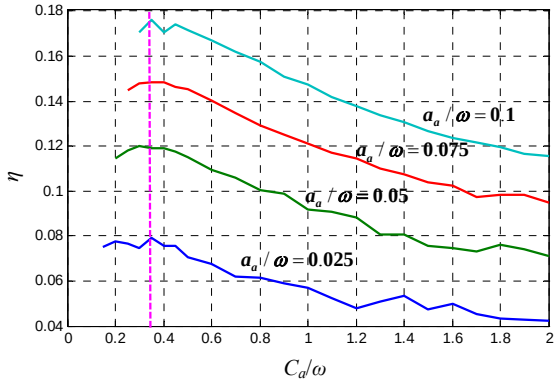

Figure 6. μa/μm=1, the calculated value of η versus Ca/ω

From Fig. 6, if μ_a/μ_m=1, i.e. the bypass core uses the same magnetic material as the main core, C_a/ω should be less than 0.4, and a_a/ω should be greater than 0.05 to ensure that η is higher than 0.12.

The value of h_a should be minimum in order to get a small length l_a of the magnetic path of the bypass core and limit leakage flux between the main core and the bypass core. This also means that the magnetic reluctance value R_a is optimized. However, the length of h_a mainly depends on the turn and the wire diameter of the bypass core winding coil.

And last, the optimal parameters of the bypass core are: $\mu_a=\mu_m$, a_a=1cm, C_a=6cm, ω=8cm, h_a=2cm, that is: μ_a/μ_m=1, a_a/ω=0.125, C_a/ω=0.75.

IV. Test Transformer Design and Platform Setup

The rated power P_{out} of the test transformer is 300W/50Hz. Considering that there will be DC-bias magnetic flux in the future test, the experience coefficient k in this transformer design could be larger than a normal transformer, thus the cross area of the main core can be calculated as,

$$S = k\sqrt{P_{out}} = 2.3\times\sqrt{300} = 40cm^2 \quad (7)$$

So, the main core is chosen as $8cm\times 5cm$.

If working magnetic flux density B_m is chosen as 0.9T,

$$N_0 = 45/(B_m S) \quad (8)$$

From equation (8), the turn per voltage N_0 is 1.25. And then the turns of the primary and the secondary winding can be derived as,

$$N_1 = N_0 U_1 = 1.25\times 220 \approx 275 \quad (9)$$

$$N_2 = \alpha N_0 U_2 = 1.05\times 1.25\times 22 \approx 29 \quad (10)$$

At last, the actual turns of the primary and the secondary winding are 300 and 30, respectively.

The diameter d of the main coil can be calculated as,

$$\pi(\frac{d}{2})^2 = I/j \rightarrow d = 1.13\times\sqrt{10/4} = 1.79mm \quad (11)$$

where I is the peak RMS current in the winding; j is the current density in the coil whose normal value varies from 2- 4A/mm2.

The core of the test transformer has four kinds of laminations with the bypass core integrated in the #1 lamination shown in Fig. 7(b). #1 lamination is made using laser cutting so as to eliminate the air gap between the bypass core and the main core. Otherwise, a much higher magnetic permeability material needs to be attached to the main core to get acceptable measurement results.

The structure of the prototype test transformer with the signal processing circuit is shown in Fig. 8.

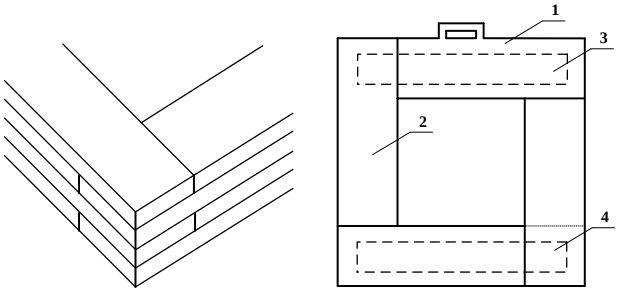

(a) lamination stack (b) laminations

Figure 7. Lamination stack and structure of the test transformer

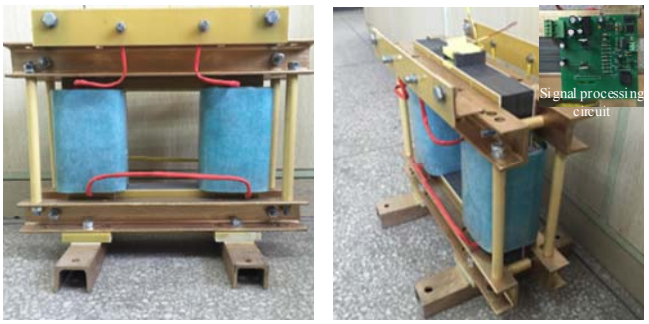

(a) test transformer (front view) (b) test transformer (side view)

Figure 8. Structure of the test transformer

The measuring circuit used in this test mainly consists of three parts: the source which generates a high-frequency signal, a current transformer and a digital filter based on EMD. High-frequency signal source is used to output signals that can be further easily separated from the 50Hz main magnetic flux frequency signals so that unwanted interferences can be reduced.

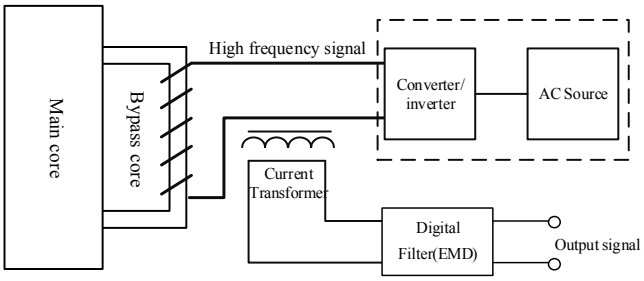

Figure 9. Measure circuit used in this test

The high-frequency signal is a square signal.

$$u = \frac{4}{\pi}\sum_1^n\left((-1)^{n+1}\frac{1}{2n-1}\cos(2n-1)\omega_h t\right) \quad (12)$$

The measured current from the current transformer is i, then L_{eq} can be calculated as,

$$L_{eq} = \frac{\Psi}{i} = \frac{\int udt}{i} \quad (13)$$

Substitute equation (12) into (13),

$$i = -\frac{4A}{\pi\omega_h L_{eq}}\sum_1^n\left((-1)^{n+1}\frac{1}{(2n-1)^2}\sin(2n-1)\omega_h t\right) \quad (14)$$

Noted that, from equation (14), it is clear that the measured current i is mainly a function of L_{eq}. If L_{eq} has a larger value range, the current i can better represent the magnetic flux in the iron cores. The measured current is transformed into voltage signals using an amplifier circuit. The test voltage waveforms are shown in Fig. 10.

As calculated in equation (9), the turn of the primary winding is 300, and the equivalent magnetic length of the main core is 1m. The output measured voltage versus magnetic strength can be calculated in the bypass coil under no DC-bias condition. Fig. 11 shows the compared waveforms of the u_L-H with the ideal BH behavior of the main core [23].

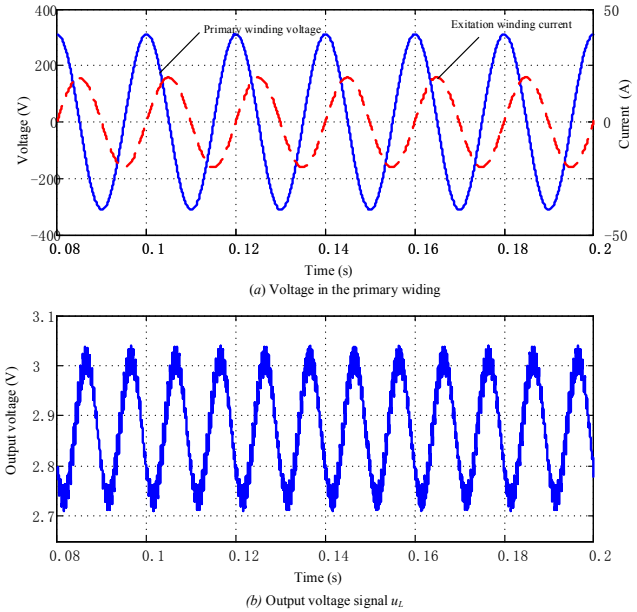

Figure 10. Waveforms of the primary winding and output voltage signal uL when there is no DC-bias current in the excitation winding

Fig. 11 shows that the out voltage of the bypass core also forms a loop which is the same with the BH curve of the actual main core. However, the measured voltage is very sensitive to the magnetic permeability of the main core. Peak values of the voltage are obtained at the point when the main core begins to enter the saturation. The highest value of the output voltage is about 3.05V and the lowest is about 2.7V. η can also be calculated from the output voltage that is about 10%, which agrees with the results shown in Fig. 5 when $\mu_a/\mu_m=1$.

When H equals zero, the output voltage on the bypass coil is the same for both the positive or negative value of the magnetic flux density. The calculated curve of the magnetic behavior can be used to determine whether there is DC-bias magnetic flux or not in the main core. If there is a DC-bias component, the curve will be asymmetry.

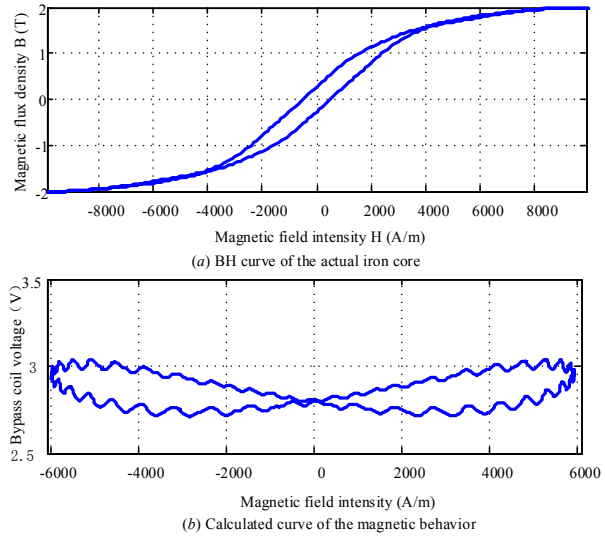

Figure 11. Comparison of the BH characterizes of the main core and the output measured voltage in the bypass coil under no DC-bias condition

As seen in Fig. 11, the output voltage contains a high-frequency noise. The max noise is about 0.06V which is 18% of the peak to peak value of the measurement. In the next section, a digital filter based on the EMD algorithm is introduced to eliminate the noise without additional analog filter circuits.

V. Measured Signal Processing

The digital filter uses the EMD algorithm to eliminate the noise in the measured signal in various applications [24-26]. EMD can decompose the basic components from the original signal; it is of no-loss and adaptive to various kinds of periodic signals in the time domain.

The algorithm flow of EMD is shown in Fig. 12：

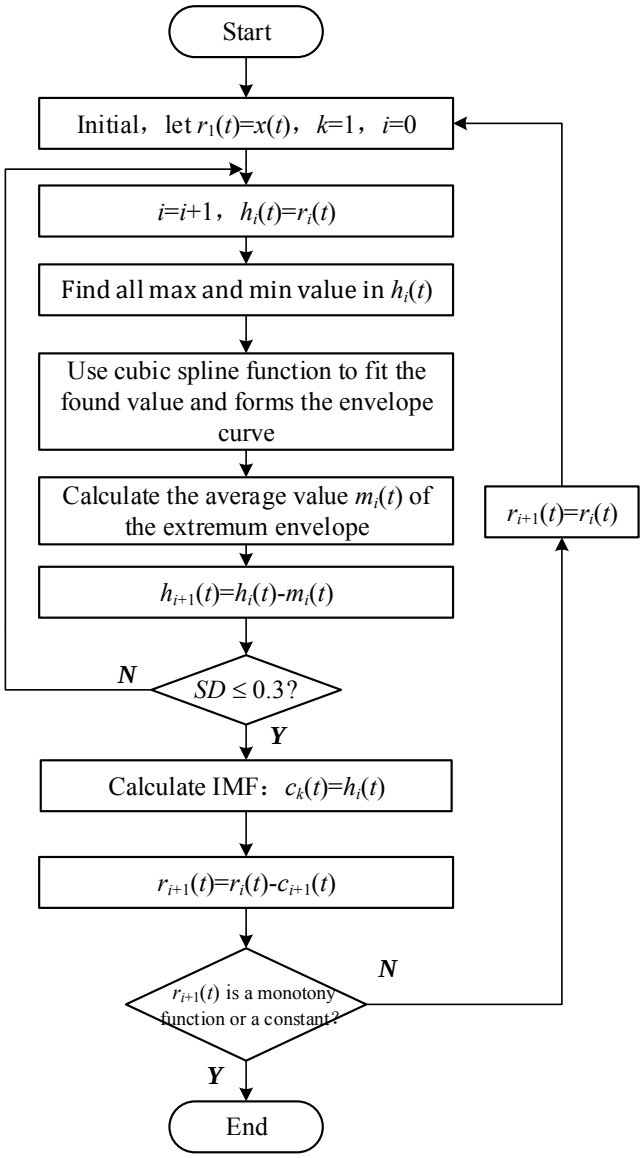

Figure 12. Flow chart of the EMD algorithm

The algorithm consists of several steps as below:

1) Define the measured signal need to be processed as $x(t)$，then find all max and min values in $x(t)$;

2) Build envelops for derived values ($x_{up}(t)$ for max values and $x_{dn}(t)$ for min values) in the first step, and then calculate the average function $m_i(t)$,

$$m_i(t)=\frac{x_{up}(t)+x_{dn}(t)}{2} \tag{15}$$

3) Calculate the intrinsic mode function (IMF) $h_i(t)$,

$$h_i(t)=x(t)-m_i(t) \tag{16}$$

If $h_i(t)$ satisfies with the condition which is shown as

follows,

$$SD = \frac{\sum[h_i(t) - h_{i+1}(t)]^2}{\sum[h_i(t)]^2} \le 0.3 \quad (17)$$

keep the calculated value of $h_i(t)$ as the new value of $x(t)$ and then go back to step 2). Use equation (15) to calculate a new value of $h_{i+1}(t)$,

$$h_{i+1}(t) = h_i(t) - m_i(t) \quad (18)$$

where i indicates the iteration number.

At last,

$$c_k(t) = h_i(t) \quad (19)$$

Calculate the residual function,

$$r_{i+1}(t) = r_i(t) - c_{i+1}(t) \quad (20)$$

where $r_1(t) = x(t) - c_1(t)$.

If $r_{i+1}(t)$ is a monotone function or a constant, the EMD calculation process ends; else let $x(t)=r_{i+1}(t)$, and then go to the start step 1).

The process results using the EMD algorithm is shown in Fig. 13. For the calculated curve of the magnetic behavior shown in Fig. 11, by using the EMD algorithm, there are 9 IMF outputs from the origin signal. As can be seen, the frequency of IMF6 is 100Hz which is the same as the signal shown in Fig. 10.

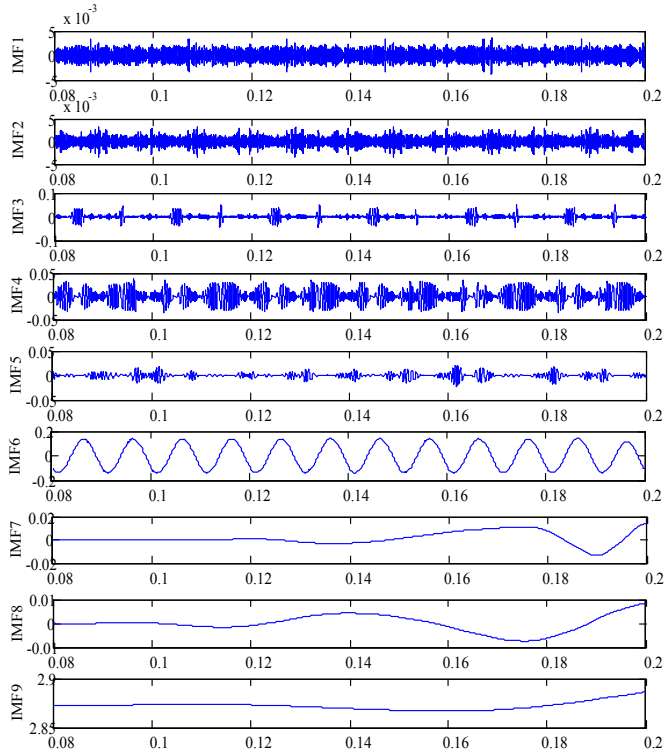

Figure 13. IMF outputs from the original signal using the EMD algorithm

After IMF1 to IMF5 are filtered, the reconstructed signal from IMF6 to IMF9 produces much less noise. As shown in Fig. 14, noises are eliminated from the curve compared with the noises in Fig. 11.

The digital filter can be further used to process the measurement of the magnetic flux when iron cores have DC components.

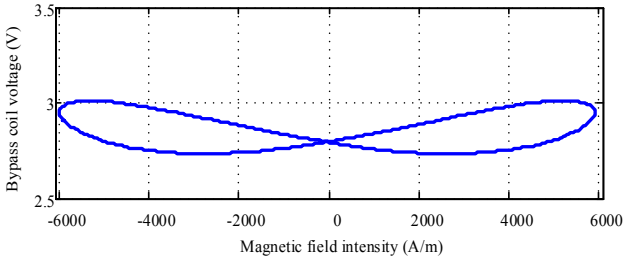

Figure 14. Reconstruct signal from IMF6 to IMF9

VI. The Measurement Results under DC-bias Conditions

Iron cores of the transformers may work in a magnetic bias state, which will make transformers output harmonics into the grids. In this section, several tests were performed to observe how magnetic flux behavior in this condition. The results can be used to verify whether the above method is correct or not.

In order to saturate the iron core of the test transformer shown in Fig. 8. DC current is injected into the excitation winding. As shown in Fig. 15, the current in the excitation winding has DC components, and its value is positive 10A. While DC current can be regulated from -10A to 10A by external controlled current source, the voltage upon the primary winding remains unchanged.

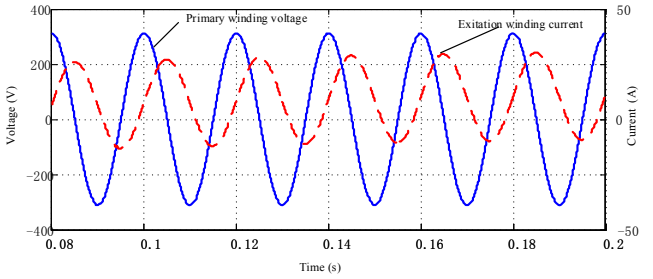

Figure 15. Waveforms of the primary winding when DC current is injected in the excitation winding

The waveforms of the original and digitally processed signal of the output voltage u_L are shown in Fig. 16.

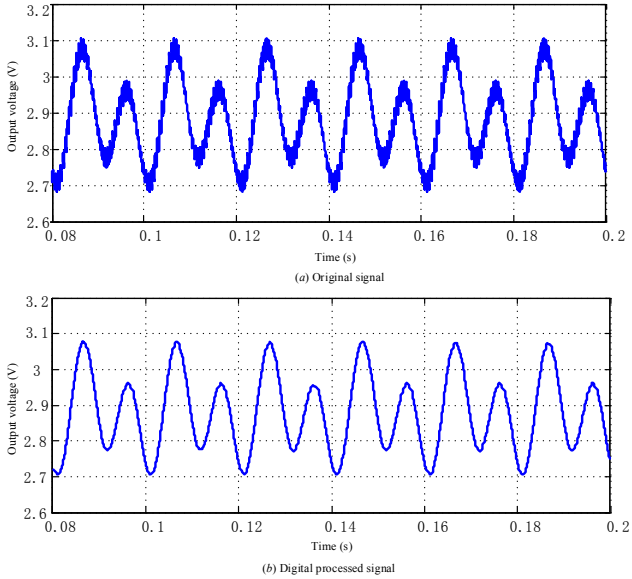

Figure 16. The output measured voltage u_L under DC-bias condition

After the noise is digitally filtered, the output signal becomes a non-sinusoidal period function versus time under DC-bias condition. There are two different peak voltages in

a period. Because the values of the magnetic permeability of the iron core are different in the liner section and the saturation section in the BH curve, the value of L_e also changes and results in asymmetric waveforms.

Fig. 17 presents the digital filtered output voltage waveforms when DC currents are 10A, 5A, -5A and -10A, respectively.

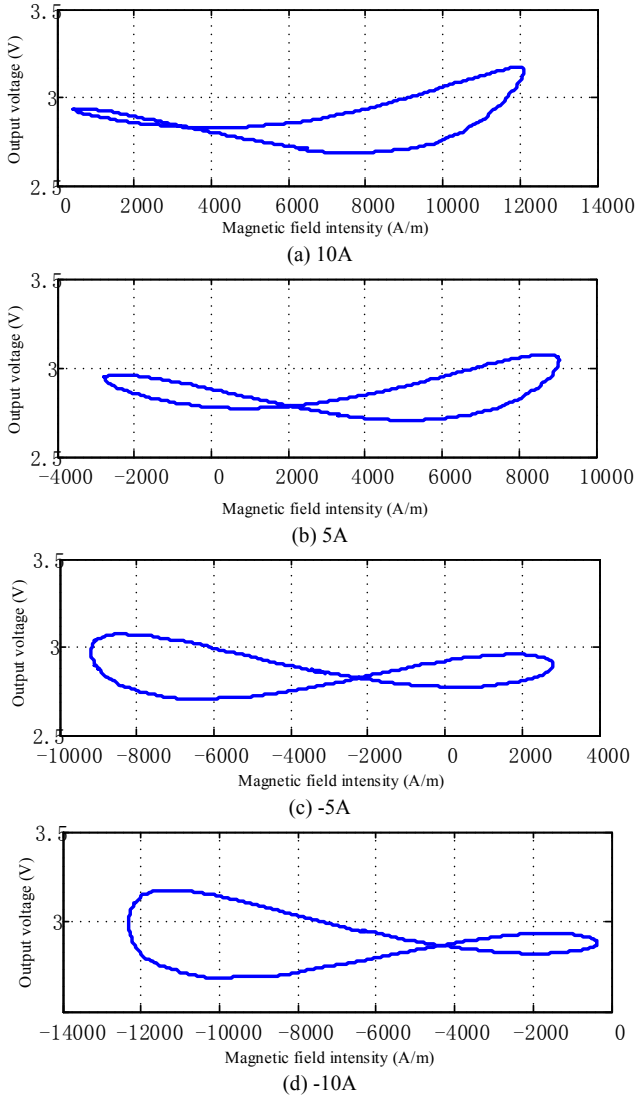

Figure 17. Waveforms of the primary winding when DC current is injected

The value of the measured voltage is considerably sensitive to the instantaneous magnetization state of the main core. From Fig. 17, it is obvious that the waveforms of the measured voltage are changed when the main core turns into saturation at different DC bias values. The peak measured voltage of the bypass core begins to increase soon after the iron cores are saturated. In Fig. 17(a), the peak value of the output voltage is 3.32V. When DC bias current decreases, the measured voltage also decreases; and the peak value is 3.19V when DC bias current is 5A as shown in Fig. 17(b). The test peak values of the measured voltages are listed in Table II.

Positive or negative DC bias current has nearly the same effect on the output voltage. However, there is a limit that the value of measured voltages can not be higher than 3.6V when DC bias current is above 30A. It is because the bypass core is deeply saturated and the magnetic flux in the shared path is limited.

TABLE II. MEASURED VOLTAGES WHEN DC BIAS CURRENTS ARE DIFFERENT

DC bias current	Measured voltages(V)
30A	3.58
20A	3.52
10A	3.32
5A	3.19
0A	3
-5A	3.19
-10A	3.35
-20A	3.51
-30A	3.59

The above test results show that the proposed method can reflect sufficient information of the dynamic magnetic flux in the main core. By further analyzing the real BH curve, accurate results can be also derived from this method.

VII. CONCLUSION

This paper proposes a real-time magnetic flux measurement of the transformers under DC biased condition by introducing a bypass iron core attached to the main iron core. Besides the addition of the bypass core, the measure device is equipped with bypass coils, high-frequency drive circuits, current transformer and output circuit with a digital filter.

The bypass core shares a partial magnetic path with the main core. In order to better represent the real-time magnetic flux, the optimal design of the core is also described so that the inductance of the coil can have a larger variation range. By injecting a high-frequency signal into this coil, the output current changes with the magnetic flux in the main core, which is transformed into a voltage signal using an amplifier circuit. The value of the measured voltage signal is considerably sensitive to the instantaneous magnetization state of the main core, and it gives sufficient information about the dynamic magnetic flux in the main core.

The method is verified, and the results show that the method can dynamically measure the BH behavior of the iron cores not only in normal operation but also in saturation condition. Because the turn number of the attached coil is much less compared with that of the main coil, there is a small voltage in the measuring circuit. Thus, the measured circuit can be further used in high voltage transformer experiments, which means that the proposed measurement has a practical significance in measuring and protecting transformers, magnetically controlled reactors, and other electromagnetic equipment.

REFERENCES

[1] V. C. Valchev , A. Van den Bossche. Inductors and transformers for power electronics. CA: CRC Press, pp:10-20, 2018.

[2] W. Xu, Y. Wu, F. Wu, X. Shen and J. Ruan, "Study on the influence factors of power transformer DC magnetic bias," in 12th IET International Conference on AC and DC Power Transmission (ACDC 2016), Beijing, 2016, pp. 1-6. doi: 10.1049/cp.2016.0416.

[3] J. Sun, J. Li, K. Wang, C. Wu, Y. Qiu and X. Yu, "Study on operating performance of transformer and scaling model with DC bias," in 2017 IEEE 26th International Symposium on Industrial Electronics (ISIE), Edinburgh, 2017, pp. 158-162. doi: 10.1109/ISIE.2017.8001240.

[4] H. Feng et al., "Analysis of Exciting Current for Single-phase Four-Limb Ultra-High Voltage Transformer Under DC Bias," in 2018

Condition Monitoring and Diagnosis (CMD), Perth, WA, 2018, pp. 1-6. doi: 10.1109/CMD.2018.8535953.

[5] Vakhnina VV, Kuvshinov AA, Shapovalov VA, Chernenko AN, Kretov DA, "The development of models for assessment of the geomagnetically induced currents impact on electric power grids during geomagnetic storms," Advances in Electrical and Computer Engineering. vol. 15, no. 1, pp.49-55, Feb. 2015.

[6] C. R. Pacheco, J. A. G. Esparza, J. G. De La Vega and R. Caraballo, "Evaluation of the Risk of Geomagnetic Induced Currents (GIC's) in Power Transformers of the National Electrical System," in 2018 XXXI International Summer Meeting on Power and Industrial Applications (Rvp-Ai), Acapulco, 2018, pp. 75-80. doi: 10.1109/RVPAI.2018.8469995

[7] Y. Xia, Y. Han and J. Liu, "Calculation of winding loss and temperature rise of large power transformer under DC magnetic biasing," in 2018 12th International Conference on the Properties and Applications of Dielectric Materials (ICPADM), Xi'an, 2018, pp. 590-593. doi: 10.1109/ICPADM.2018.8401087.

[8] D. Xia, "The Distribution of Transient Magnetic Field and Eddy Current Losses of Three-Phase Five-Legged Transformer Under DC Bias," in 2018 IEEE International Conference on Internet of Things (iThings) and IEEE Green Computing and Communications (GreenCom) and IEEE Cyber, Physical and Social Computing (CPSCom) and IEEE Smart Data (SmartData), Halifax, NS, Canada, 2018, pp. 728-732. doi: 10.1109/Cybermatics_2018.2018.00145.

[9] X. Song, B. Zhou and L. Wang, "Transient Eddy Current Loss and Magnetic Field Distribution of Single-phase Three-legged Transformer under DC Bias," in 2018 13th World Congress on Intelligent Control and Automation (WCICA), Changsha, China, 2018, pp. 1053-1057. doi: 10.1109/WCICA.2018.8630589.

[10] H. L. Weng, L. Liu, Y. Wan, X. N. Lin, Z. X. Li and J. G. Huang, "Studies on the Variation of Transformer Reactive Power Caused by DC Bias and Its Impacts on System Voltage," in 2018 IEEE International Conference on High Voltage Engineering and Application (ICHVE), ATHENS, Greece, 2018, pp. 1-4. doi: 10.1109/ICHVE.2018.8641961

[11] Y. Xu, M. Dai and W. Wang, "An Analysis of Transformer Core Vibration and Noise Under DC Bias Condition," in 2017 International Conference on Computer Systems, Electronics and Control (ICCSEC), Dalian, 2017, pp. 1612-1615. doi: 10.1109/ICCSEC.2017.8446974.

[12] J. Liu and L. Luo, "Noise characteristics of the new converter transformer under DC bias," Electronics Letters, vol. 53, no. 10, pp. 672-674, 11 5 2017. doi: 10.1049/el.2017.0610.

[13] J. Horiszny, "Method of determining the residual fluxes in transformer core," in 2017 18th International Symposium on Electromagnetic Fields in Mechatronics, Electrical and Electronic Engineering (ISEF) Book of Abstracts, Lodz, 2017, pp. 1-2. doi: 10.1109/ISEF.2017.8090688.

[14] B. Tanatarec, "Measurements of magnetic flux density in the vicinity of transformer station," in 2016 22nd International Conference on Applied Electromagnetics and Communications (ICECOM), Dubrovnik, 2016, pp. 1-4. doi: 10.1109/ICECom.2016.7843903.

[15] W. Jiang, L. He and Z. X. Zhang, "Monitoring and suppression measures of transformer DC bias current," in 2016 International Conference on Condition Monitoring and Diagnosis (CMD), Xi'an, 2016, pp. 364-367. doi: 10.1109/CMD.2016.7757873.

[16] M. Kazerooni and T. J. Overbye, "Transformer Protection in Large-Scale Power Systems During Geomagnetic Disturbances Using Line Switching," IEEE Transactions on Power Systems, vol. 33, no. 6, pp. 5990-5999, Nov.2018. doi: 10.1109/TPWRS.2018.2830333.

[17] British Standard, "Magnetic Materials-Part 2: Methods of measurement of the magnetic properties of electrical steel sheet and strip by means of an Epstein frame", BS EN 60404–2:1998, IEC 404–2: 1996.

[18] H. Huang, B. Wei, L. Su, W. Zhao, X. Zhang and X. Zheng, "Study on Technical Standards of Direct Current Bias Magnetic Suppression Device of Power Transformer," in 2018 IEEE International Power Electronics and Application Conference and Exposition (PEAC), Shenzhen, 2018, pp. 1-4. doi: 10.1109/PEAC.2018.8590370.

[19] D. Chen, Z. Feng, Q. Wang, L. Fang and B. Bai, "Study of Analysis and Experiment for Ability to Withstand DC Bias in Power Transformers," IEEE Transactions on Magnetics, vol. 54, no. 11, pp. 1-6, Nov. 2018, Art no. 8401406. doi: 10.1109/TMAG.2018.2844208.

[20] J. Yuan et al., "A Novel Compact High-Voltage Test System Based on a Magnetically Controlled Resonant Transformer," IEEE Transactions on Magnetics, vol. 51, no. 11, pp. 1-4, Nov. 2015, Art no. 1700204. doi: 10.1109/TMAG.2015.2449336.

[21] L. Bowei, M. Hai and Z. Lixing, "On-Line Monitoring of Transformer Vibration and Noise Based on DC Magnetic Bias," in 2013 Fourth International Conference on Intelligent Systems Design and Engineering Applications, Zhangjiajie, 2013, pp. 412-416. doi: 10.1109/ISDEA.2013.498.

[22] X. Chen, Z. Wang and B. Wang, "Research on Dynamic Magnetic Flux Measurement Under DC-Biased Magnetization by the Type-c Transducer," IEEE Transactions on Magnetics, vol. 51, no. 11, pp. 1-4, Nov. 2015, Art no. 6101304. doi: 10.1109/TMAG.2015.2436894.

[23] Valentin Ionita, Lucian Petrescu, Adelina Bordianu and Octavian Tabara, "Efficient Use of Preisach Hysteresis Model in Computer Aided Design," Advances in Electrical and Computer Engineering, vol. 13, no. 2, pp.121-126, May. 2013. doi:10.4316/AECE.2013.02019

[24] Y. Kopsinis and S. McLaughlin, "Development of EMD-Based Denoising Methods Inspired by Wavelet Thresholding," IEEE Transactions on Signal Processing, vol. 57, no. 4, pp. 1351-1362, April 2009. doi: 10.1109/TSP.2009.2013885.

[25] S. Shukla, S. Mishra and B. Singh, "Power Quality Event Classification Under Noisy Conditions Using EMD-Based De-Noising Techniques," IEEE Transactions on Industrial Informatics, vol. 10, no. 2, pp. 1044-1054, May 2014. doi: 10.1109/TII.2013.2289392.

[26] L. Wang, H. Chen, S. Li, X. Chen and W. Wang, "Wavelet threshold analysis combined with EMD method for mechanical equipment fault diagnosis," in 2017 36th Chinese Control Conference (CCC), Dalian, 2017, pp. 5060-5063. doi: 10.23919/ChiCC.2017.8028155